From models to mechanisms: defects and charge trapping in amorphous silicon nitride

Hückmann, L.

Citation

Hückmann, L. (2026, July 2). *From models to mechanisms: defects and charge trapping in amorphous silicon nitride*. Retrieved from https://hdl.handle.net/1887/4307230

Version:	Publisher's Version
License:	Licence agreement concerning inclusion of doctoral thesis in the Institutional Repository of the University of Leiden
Downloaded from:	https://hdl.handle.net/1887/4307230

Note: To cite this publication please use the final published version (if applicable).

6

From Jekyll to Hyde and Beyond: Hydrogen's Multifaceted Role in Passivation, H-Induced Breakdown, and Charging of Amorphous Silicon Nitride

This chapter is based on

Cottom, J.; **Hückmann, L.**; Olsson, E.; Meyer, J. "From Jekyll to Hyde and Beyond: Hydrogen's Multifaceted Role in Passivation, H-Induced Breakdown, and Charging of Amorphous Silicon Nitride" *J. Phys. Chem. Lett.* **2024**, *15*, 840–848.

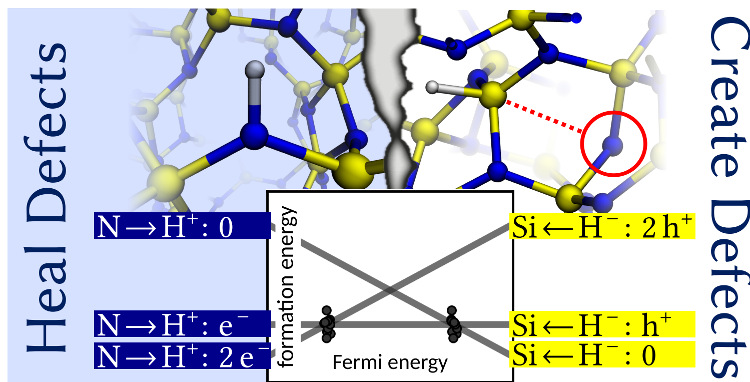

THE JOURNAL OF
PHYSICAL CHEMISTRY
LETTERS
A JOURNAL OF THE AMERICAN CHEMICAL SOCIETY

January 25, 2024
Volume 15
Number 3
pubs.acs.org/JPCL

ACS Publications
Most Trusted. Most Cited. Most Read.

www.acs.org

Abstract

In semiconductor devices, hydrogen has traditionally been viewed as a panacea for defects, adept at neutralizing dangling bonds and consequently purging the related states from the band gap. With amorphous silicon nitride (a-Si_3N_4) — a material critical for electronic, optical, and mechanical applications — this belief holds true as hydrogen passivates both silicon and nitrogen dangling bonds. Yet, there is more to the story. The presented density functional theory calculations unveil hydrogen's multifaceted role upon incorporation in a-Si_3N_4. On the "Jekyll" side, hydrogen atoms are indeed restorative, healing coordination defects in a-Si_3N_4. However, "Hyde" emerges as hydrogen induces Si—N bond breaking, particularly in strained regions of the amorphous network. Beyond these dual roles, this chapter reveals an intricate balance between hydrogen defect centers and intrinsic charge traps already existing in pristine a-Si_3N_4: The excess charges provided by the H atoms result in a charging of the a-Si_3N_4 dielectric layer.

6.1 Introduction

Silicon nitride has been a technologically important material for a number of years due in no small part to its attractive chemical, mechanical and electronic properties. This has led to it being deployed in a broad range of applications covering wear resistant coatings,[1] electronic devices (MOSFETs and MEMs),[2,3] high energy optics,[4–6] integrated photonics,[7,8] and lithography.[9–11] For a small number of applications silicon nitride is used in the crystalline phase.[12,13] However, in most use cases it is deployed as an amorphous thin film (a-Si_3N_4).[3,14–19] The addition of hydrogen can be intentional, as is the case with photovolatics and electronic devices, that undergo an H-anneal step. This passivation step has been shown to be both a blessing, passivating dangling bonds,[20–22] and a curse, affecting structural stability and altering the charge trapping properties.[23–26] Alternatively, H can be incorporated unintentionally as a result of exposure to the environment, such as is the case in lithography.[4–6,9–11,27] Finally, a certain concentration of H will be incorporated from

the precursors during thin film growth by chemical vapor deposition, typically SiH_4 and its derivatives. Regardless of how H is introduced to a-Si_3N_4, at the atomic scale understanding of H-incorporation and the concomitant modification of the material's properties has not been established.

Notwithstanding, experimental and theoretical studies have provided a number of important insights. H-defects have been linked to the passivation of dangling bonds within the a-Si_3N_4 network,[20–22,28–38] based on a reduction of the observed concentration of paramagnetic centers upon increase in Si–H vs. N–H concentration.[39,40] In addition, the post-deposition treatment with H leads to significant changes in the observed photoluminescence and EPR spectra.[26,41,42] The latter results suggest that H plays a dual role, leading to a reduction in mid-gap recombination centers while favoring or introducing others, resulting in both radiative and non-radiative recombination pathways.[26] Conversely, it has been observed that as the H concentration in the a-Si_3N_4 film increases, the temperature stability of the film decreases.[24,25,43,44] The disparate nature of H-incorporation on the properties of a-Si_3N_4 suggests a range of atomic environments beyond just the passivation of dangling bonds to be of relevance.

H-incorporation in a variety of wide band-gap oxides has been extensively studied.[45–54] Therefore, it is tempting to look for parallels between nitrides and oxides. In particular, the interaction of H with SiO_2 shows a number of similar trends as for a-Si_3N_4 summarized above, reducing the number of coordination defects while forming new defect centers.[52–55] The formation of new defect centers and the disruption of the silica lattice are suggested to result in the observed hydrolytic weakening, whereby exposure to H_2 and H_2O induces a significant weakening in SiO_2 and a-Si_3N_4.[43,44,56,57] Theoretical studies have provided atomistic insights into H incorporation in SiO_2 and identified a mechanism for the H-induced bond breaking.[52–55] In general, for a broad range of oxides, H-defects fit into two main categories. The first category are amphoteric defects, which result in H-states deep in the band-gap and typically exhibit negative-U character, whereby the charge state (+/−) is dictated by the Fermi energy in the device. Alternatively, H can act as an n-type dopant introducing states in the vicinity of the conduction band minimum (CBM). A link between the (+/−) H charge transition level (CTL) and a universal value has been postulated, which further is related to the charge neutrality level (3.0 eV,[49] 3.9 eV,[51] and 4.5 eV[48] below the vac-

uum level depending on the electronic structure approach employed), Li and Robertson[51] noted that this description and the concomitant universal value breakdown when the H is able to form a dative bond with the O-site. Considering the fact that chemical bonding in a-Si_3N_4 is markedly different compared to a-SiO_2, it is an open question if (and if so how) the aforementioned prevalent description of H defects can be extended to this class of material.

Here I present a systematic study of H incorporation in a-Si_3N_4 as a function of the local atomic environment. To ensure a statistically meaningful range of H-incorporation sites are considered, the sampling scheme presented in Chapter 3 is adapted to study the stability, structural features, charging behavior and interplay between the extrinsic H-defects and intrinsic charge trapping as characterized in Chapter 5. This allows to quantify the multifaceted role H plays in a-Si_3N_4, including passivation, and the hitherto unknown structural modifications and H-induced breakdown of the network. The results underscore a pronounced interplay between H and existing charge traps within the amorphous network. This nuanced behavior finds its roots in semi-localized states proximate to the CBM and VBM, resulting in an electrically inactive H-center. Upon the incorporation of charge donated by hydrogen, the excess charge is then localized at intrinsic traps.

6.2 Results and Discussion

6.2.1 Hydrogen Incorporation in β-Si_3N_4

The incorporation of hydrogen in the most stable crystalline phase (β-Si_3N_4) has been studied by Di Valentin *et al.*[33] and Grillo *et al.*[58] To ensure the comparability between the results presented here and those from previous work as well as to facilitate the transferability between the crystalline and the amorphous phase, H interstitials in β-Si_3N_4 are briefly revisited.

The structure of β-Si_3N_4 can roughly be described as layers of eight- and twelve-membered rings in the [110]-plane which are interlinked in [001]-direction such that they form narrow and wide tubes along the [001]-axis, see Section 2.1. This leads to two distinct H-incorporation sites in the wide and in the narrow ring each as shown in Figure 6.1a and b. At both sites, hydrogen forms a negative-U amphoteric defect ($U \approx -0.5$ eV) familiar from a

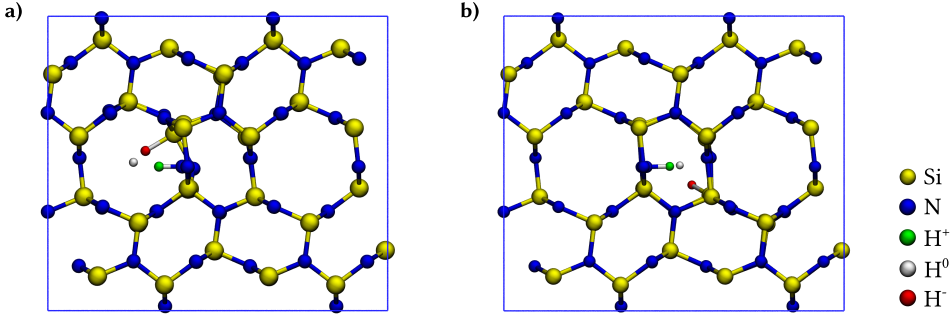

Figure 6.1: Schematic representation along the [001] direction of the two H-incorporation sites in β-Si_3N_4 with a) H in the wide ring and b) H in the narrow ring. Hydrogen atoms in the positive charge state are colored green, the ones in the neutral charge state are white, and the ones in the negative charge state are red. For computational ease, the structure is extended into an orthogonal box containing 280 atoms.

broad range of oxides,[48,51] most notably SiO_2 meaning that depending on the Fermi energy either the H^+ or H^- is favored. At $E_F < 3.28$ eV the H^+ is favored, sitting at a N-site with an N–H separation of 1.05 Å, while above 3.28 eV the H^- is more stable, sitting adjacent to a Si with a separation of 1.5 Å. Finally, while never energetically favored, in the neutral charge state, the H adopts an interstitial configuration. This maximizes the distance to the neighboring ions, resulting in a Si/N–H separation of 2.4 Å. The (+/−) CTL sits approximately 4.15 eV below the vacuum level and in reasonable agreement with the observations of van de Walle and Neugebauer[48] as well as Li and Robertson.[51] Remarkably and in contrast to the crystalline system, the non-interacting H^0 interstitial does not form in a-Si_3N_4. Instead, both N and Si-centered H defects are found and discussed below, starting from the neutral charge state in both cases.

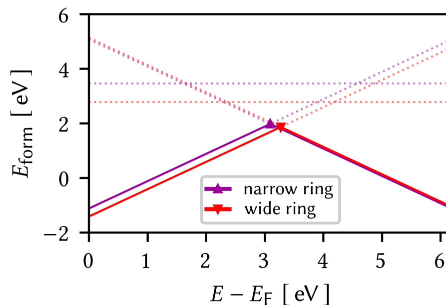

Figure 6.2: Formation energies E_{form} as a function of the Fermi level E_F for the hydrogen defect sites in the narrow (purple) and in the wide rings (red) in the +1, neutral, and −1 charge states.

6.2.2 N–H Defects in a-Si_3N_4

Two main types of N–H defects are dictated by the original coordination of the reference site in the precursor geometry (Figure 6.3a, b):

1. H-incorporation on 2-coordinated N resulting in a passivation type interaction ($Si_2N–H_{pass}$), and
2. H-incorporation on 3-coordinated N resulting in a tetrahedral-like distortion of the planar N forming a hydrogen interstitial ($Si_3N–H_{i\text{-}N}$).

The N–H bond lengths for both cases sit in a tight range between 1.01 Å to 1.06 Å with one outlier at 1.10 Å and the mean at 1.03 Å (Figure 6.3c). This makes the bonds marginally elongated compared to N–H bond length in ammonia.[59] As to be expected, the very few H_{pass} defects present in the cell form the closest match and also come with the most favorable formation energies as shown in Figure 6.3d. Again for both H_{pass} and $H_{i\text{-}N}$, incorporation coincides with negligible structural relaxation as the adjacent N–Si bonds lengthen only by 0.11 Å (≈ 6 %) on average. In contrast, the formation energies in the neutral charge states (E^0_{form}) for $H_{i\text{-}N}$ extend over a considerable range 0.68 eV to 3.27 eV (see Figure 6.3d). The fact that the $H_{i\text{-}N}$ sites are uniform in terms of N–H bond length and coordination geometry of the N-host indicates that the local environment of the host site dictates E^0_{form}. This is confirmed in Figure 6.3e, illustrating that E^0_{form} scales with the local steric environment, described by the Voronoi volume (V_{Voro}) of the incorporation site. In general , a high degree of steric crowding (small V_{Voro}) results in high E^0_{form} and a small steric crowding (large V_{Voro}) low E^0_{form}. Sites with a nitrogen atom opposite to the host atom lead to a bridge-like interaction (N–H···N,). The H···N distance is between 1.68 Å to 1.85 Å with an N–H···N angle between 147.4° to 178.7° These structural arrangements allow H incorporation in sterically crowded regions of the lattice with a reduced energetic penalty (filled squares in Figure 6.3e). Finally, a subset of $H_{i\text{-}N}$ defects can be distinguished which creates new states for electron trapping that are not present in the pristine cell (*vide infra*). As illustrated by the filled diamonds in Figure 6.3e, this subset follows the aforementioned trend less clearly.

Consideration of the +1 and −1 charge states show that the H geometry is decoupled from the charge state with no change in neither N–H bond length nor orientation. The reason for

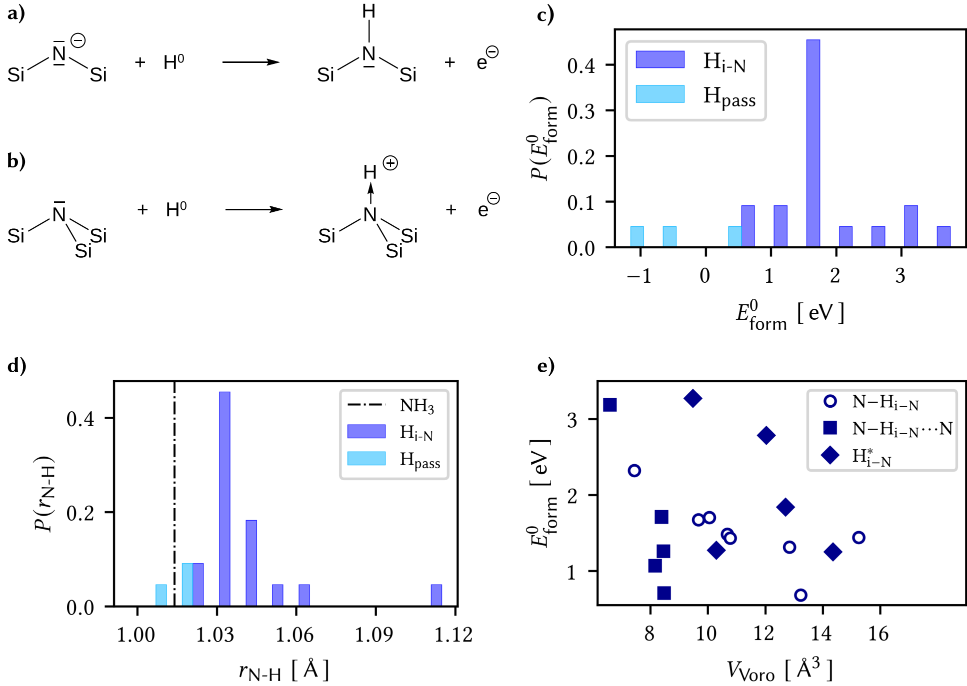

Figure 6.3: Schematic representation of N−H defect configurations on 2- and 3-coordinated host atoms forming a) H passivation sites (H_{pass}) and b) H interstitial sites ($H_{i\text{-}N}$) in the neutral charge state ($q = 0$). The excess electron of the neutral hydrogen atom (H^0) is detached from the site and trapped at an intrinsic defect in the material. c) Distribution P of the N−H bond lengths for H_{pass} (light blue) and $H_{i\text{-}N}$ (dark blue). For comparison, the N−H bond length of ammonia (NH_3) is indicated as the dashed-dotted line.[59] d) Distribution P of the formation energies E^0_{form} (same color code as in c). e) E^0_{form} as a function of the Voronoi volume V_{Voro} for $H_{i\text{-}N}$. This group of defects is further decomposed into different subgroups: Interstitials with a hydrogen bridge-like site N−$H_{i\text{-}N}$···N, which are marked as squares (28 %). Those inducing new electron trap sites not present in the pristine cell (H^*_{iN}) are marked as diamonds (23 %). The remainder (49 %), where H interacts with a single N and the electron is trapped at the original H-free trap site, are labeled by N−$H_{i\text{-}N}$ and marked as empty circles.

this becomes apparent by examining the electronic density of states (DOS) in the neutral charge state shown in Figure 6.4a for a representative configuration. The H-related electronic states are smeared out with no significant contribution to the DOS below the VBM and empty states ≈ 1.0 eV above the CBM, respectively. As there are no H-states within the band gap, H−N are electronically inactive, and the charge state of H is thus independent of the device Fermi level — unlike for amphoteric H defects. Instead, H is datively bound to N resulting in a H^+ character. The excess electron provided by the hydrogen is localized at an intrinsic trap site at a strained SiN_4 tetrahedron as previously identified and character-

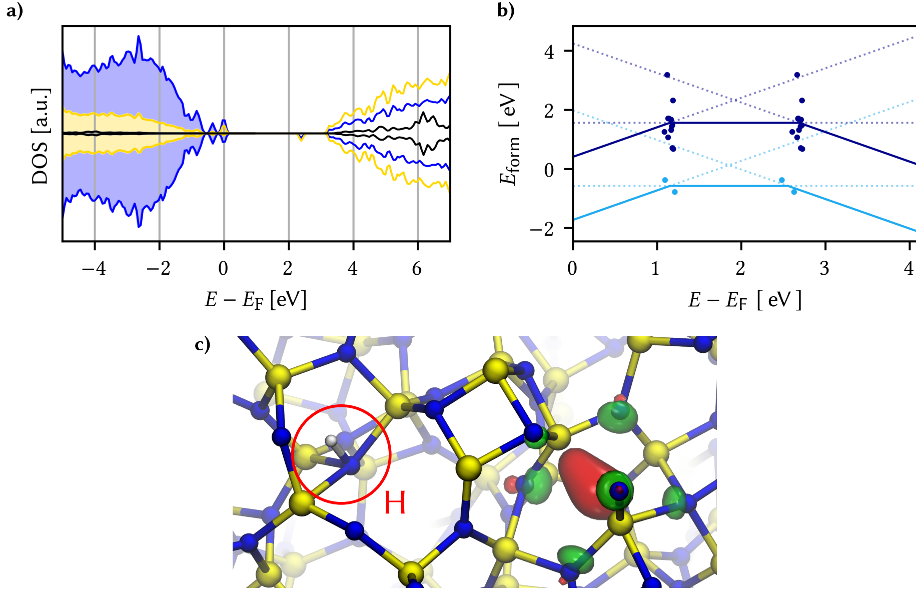

Figure 6.4: a) Projected electronic density of states (DOS) of Si (yellow), N (blue), and H (black) in a single representative neutral $H_{i\text{-}N}$ configuration relative to the Fermi level E_F. The DOS of H is amplified by a factor of 50 for visibility. b) Formation energies E_{form} as function of the Fermi level E_F for the H_{pass} and $H_{i\text{-}N}$ defects in the +1, neutral and −1 charge states (same color code as in Figure 6.3f). Solid lines mark the average over the entire ensemble, points indicate the individual +1/0 (average 1.2 eV) and 0/ − 1 (average 2.6 eV) charge transition levels. Samples inducing new electron trap sites not present in the pristine cell (H^*_{iN} in Figure 6.3e) are not included. c) Representative example of the localized state on a Si atom formed independently from the N–H site in the neutral charge state. Si is colored in yellow, N is blue, and H is white. The respective spin channels are colored red and green.

ized in Chapter 5. For the majority of cases (77 %, N–$H_{i\text{-}N}$ and N–$H_{i\text{-}N}$···N), the spin density, Mulliken charge, and DOS reveals an unpaired electron localizing consistently on the same intrinsic trap site within the cell as illustrated in Figure 6.4b. The fact that charge trapping is thus dominated by a feature of pristine a-Si_3N_4 rationalizes the lack of geometric relaxation of H defects upon charging, and the extremely small spread of the CTLs shown in Figure 6.4c. Both are distinct features of H incorporation enabled by the dative bonding and clearly at odds with amphoteric H defects. In the remaining cases (23 % H^*_{iN}, not considering H_{pass}), the structural distortion caused by the H incorporation induces an alternative precursor site, centered on a single distorted Si tetrahedron where the electron localizes. In both cases, this intimate link between effectively adding or removing charges and structural relaxation is equivalent to intrinsic charge trapping in the H-free cell. It is important to note that in the −1 charge state both electrons occupy the trap state forming a bi-polaron. The

local structure of the trap site experiences pronounced relaxation resulting in a breaking of the Si–N ($\Delta r_{\mathrm{SiN}} = 0.55$ Å), and the Si is back-projected in such a way that it interacts with an adjacent Si neighbor. Nevertheless, the Si–Si distance is 2.26 Å and the structure is similar to the $N_3Si{-}SiN_{x\in\{3,4\}}$ previously described in Chapter 5.

6.2.3 Si–H Defects in a-Si_3N_4

For the H defects interacting with Si, three main classes of defects have been identified as outlined in Figure 6.5a-c:

6

a) H interacting with a single fully coordinated Si atom ($N_4Si{-}H_{\text{i-Si}}$),

b) H bridging between two adjacent Si atoms, in addition to their regular link via a N atom in the a-Si_3N_4 network ($N_4Si{-}H_{\mathrm{bri}}{-}SiN_4$),

c) H inserting across a strained Si–N bond resulting in H–SiN_3 and an adjacent 2-coordinated N ($N_3Si{-}H_{\mathrm{ins}}$).

The Si–H bond lengths spread over a range from 1.40 Å to 1.69 Å (Figure 6.5d), with the $H_{\text{i-Si}}$ and H_{bri} configurations being significantly elongated compared to the Si–H bond length in silane (1.48 Å).[60] On average they measure 1.53 Å and 1.59 Å, respectively. The H_{bri} bonds are shifted to higher values as they are shared between adjacent Si atoms. In both configurations the coordination shell of the Si remains intact. In contrast, the H_{ins} sites show a dramatic elongation of one of the Si–N bonds with a mean separation of 2.75 Å post relaxation, while the Si–H bond relaxes to 1.47 Å on average, approximately the same length found in the silane see Figure 6.5d. The range of Si–H bond lengths are dictated by the local environment, impacting how the H is incorporated initially and subsequently how the defect center is able to relax. As schematically depicted in Figure 6.5c, H-insertion occurs via backside insertion on the SiN_4 tetrahedra so that the opposing Si–N bond is broken while the Si-center back-projects. The relaxation bears similarities to the "puckering" described for oxygen vacancies in a-SiO_2,[55,61] albeit with some important differences as the relaxation drives the breaking of a Si–N bond, and is restricted due to the lack of flexibility imparted by 3-coordinated N-anions. This is in contrast to H-induced bond rupture found in SiO_2

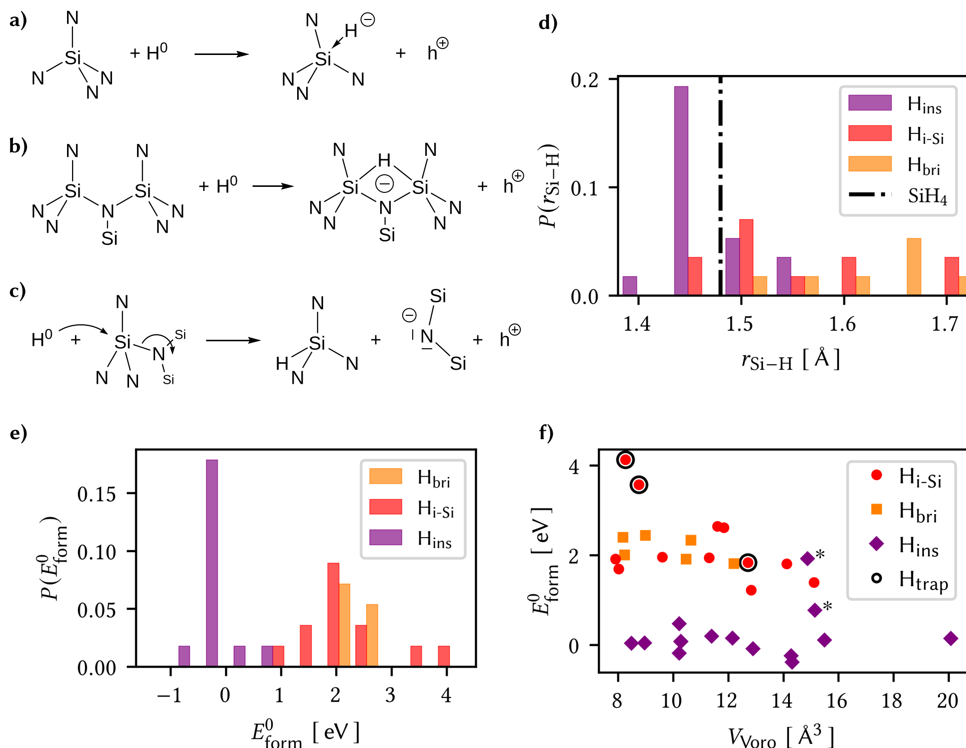

Figure 6.5: Schematic representation of Si–H defect configurations in the neutral charge state ($q = 0$) with a) H interstitial sites ($H_{i\text{-}Si}$), b) bridging H sites (H_{bri}), and c) H insertion sites (H_{ins}). The electron deficit to form a Si–H bond is compensated by taking an electron from the valence band, inducing a hole polaron (h^+) at a site uncorrelated with the H-defect. d) Distribution P of the Si–H bond length with $H_{i\text{-}Si}$ (red), H_{bri} (orange), and H_{ins} configurations (dark red). For comparison, the Si–H bond length of silane (SiH_4) is indicated by the dashed-dotted line.[60] e) Distribution P of the formation energies E^0_{form} (the same color scheme as in d). f) E^0_{form} as a function of the Voronoi volume V_{Voro} for the configurations $H_{i\text{-}Si}$ (hollow circles), H_{bri} (squares), and H_{ins} (diamonds). There are three cases marked with black circles (H_{trap}), which have a notably different electronic structure causing H-induced trapping, as further discussed in the text.

where insertion is driven by interaction with the O-site resulting in the hydroxylated E′ center ($O_3Si{-}OH$ + $^*SiO_3$).[53,54]

In terms of formation energy E^0_{form}, the Si–H defects extend over a wide range between −0.39 eV to 4.13 eV (Figure 6.5e). The energy range can be further grouped by the incorporation modes as shown in Figure 6.5e and f: Analogous to interstitial sites centered on nitrogen, $H_{i\text{-}Si}$ scales with the local steric environment (V_{Voro}), where regions with low steric repulsion (large V_{Voro}) are favored over sterically crowded regions (small V_{Voro}). Furthermore, in common with N–H centers, interaction with a neighboring Si atom results in stabiliza-

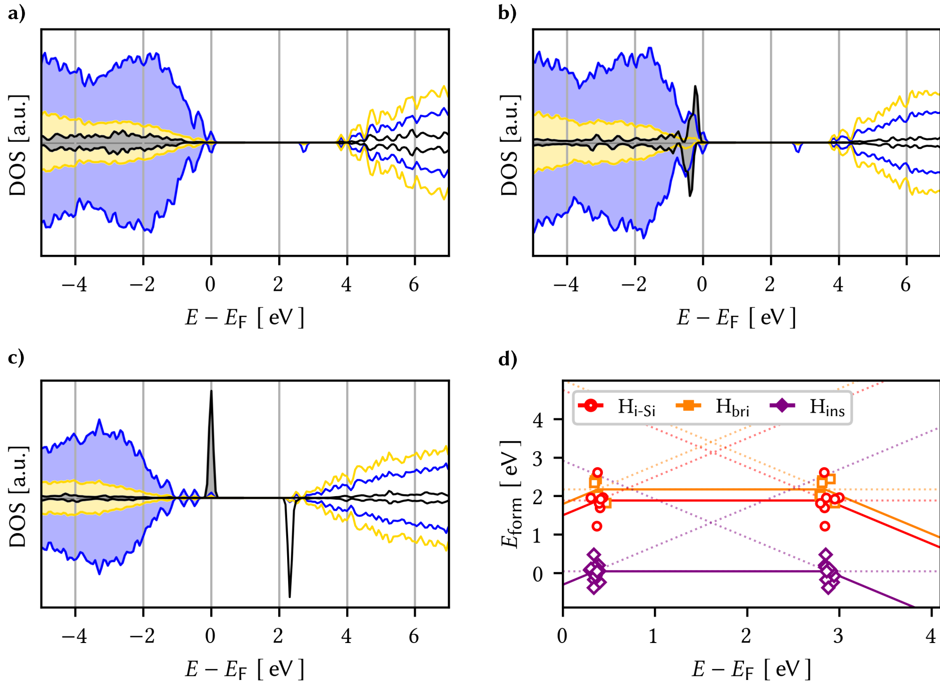

Figure 6.6: a)-c) Projected electronic density of states (DOS) of Si (yellow), N (blue), and H (black) relative to the Fermi level E_F. The DOS of H is amplified by the factor of 50 for visibility. a) and b) show DOSs for individual configurations representative for H_{ins} and H_{bri}, respectively. c) shows an exceptional $H_{i\text{-}Si}$ configuration where no proper Si–H bond could be formed. This results in a single electron being localized on the H atom while not inducing a hole polaron in the bulk as depicted in Figure 6.5a). d) Formation energies E_{form} as a function of the Fermi level E_F for the $H_{i\text{-}Si}$, H_{bri}, and H_{ins} defects in the +1, neutral, and −1 charge states (same color code as in Figure 6.5f). Solid lines mark the average over the entire ensemble together with the individual data points for the +1/0 (average 0.4 eV) and 0/ − 1 (average 2.9 eV) charge transition levels.

tion of the H_{bri} configurations. It is interesting to note that there are 2-intermediate configurations identified, where the local environment frustrates the relaxation to H_{ins}, resulting in an H–$SiN_3 \cdots$N type configuration (Figure 6.5f indicated with an asterisk). In addition and as indicated in Figure 6.5f by black circles, there are three $H_{i\text{-}Si}$-like cases that are electronically distinct as further analyzed below. In contrast, for H_{ins} sites a different picture emerges: E^0_{form} sits in a tight range between −0.39 eV to 0.77 eV with the mean at 0.11 eV, with a small number of outliers at higher energy where the local geometry frustrates the relaxation. E^0_{form} is largely independent of both the local steric environment, being driven by the H-insertion.

Focusing on the majority of the Si–H configurations, the corresponding +1 and −1 charge states turn out to leave the H incorporation geometry unchanged — just as observed for the N-centered H defects above. The reason for this is illustrated by the DOSs shown in Figure 6.6a and b for H_{ins} and H_{bri}, respectively. The H-states sit above the CBM (H_{ins}) and below the VBM (H_{bri}), resulting in an electrically inactive H-center. The charge trapping in the system is mediated by h^+ trapping on 2-coordinated N as previously described in Chapter 5. For H_{ins}, the formation of the Si–H and creation of the 2-coordinated N^0 results in the relaxation of the h^+ to the lowest energy trap site. In the $H_{i\text{-}Si}$ and H_{bri} the H is bound to one or more Si, resulting in a H^- character quantified by a Mulliken charge of $-0.1\ e$ in line with the trend from H^--cation interaction observed in oxides. The formation of H^- is driven by the H states sitting below the VBM resulting in the neutral charge state $Si + H^0 \longrightarrow Si{\leftarrow}H^- + h^+$. In each case the hole is localized on the same 2-coordinated N, which was the previously identified hole trapping site in the H-free case. Analogously to the N-centers, charge trapping is thus dominated by a feature of pristine a-Si_3N_4, and rationalizing the very small spread of the CTLs shown in Figure 6.6d as a consequence.

6

Returning to those $H_{i\text{-}Si}$ configurations which are marked in Figure 6.5f by black circles. Based on their geometry, the H atom appears to interact with a single Si atom only in those cases. However, the representative DOS shown in Figure 6.6c and the charged counterparts of these configurations reveal something quite different, namely that in all of those cases H-induced traps form. These traps are formally in the neutral charge state (H^0) with the frontier states both H in nature. This is the reason why they show the negative-U (close to $U = 0$) behavior with a charge-dependent structural relaxation of the incorporated H atoms as extensively described for amphoteric hydrogen defects in wide band-gap oxides, see Figure 6.7.

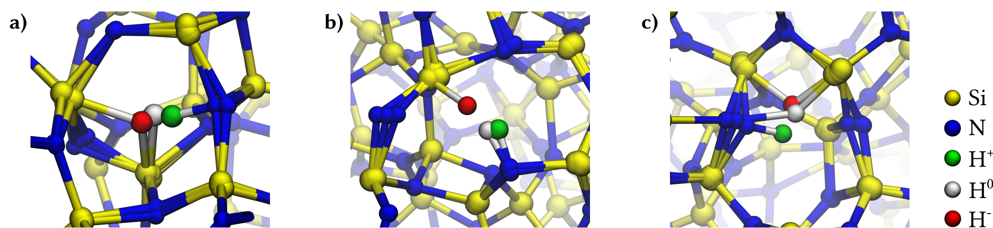

Figure 6.7: a)-c) Illustration of the charge-dependent structural relaxation for these three cases. Hydrogen is colored according to the charge state of the system in green ($q = +1$), white ($q = 0$), and red ($q = -1$), Si is colored blue and N is yellow.

6.2.4 Discussion

H-incorporation in a-Si_3N_4 is rich and notably different from what has been previously described for crystalline β-Si_3N_4, where formation of negative-U amphoteric defect centers dominates and analogous to observations in a broad range of wide band gap oxides. Table 6.1 provides a schematic overview for a-Si_3N_4 including their charge dependence, which is discussed further in the following.

In agreement with previous work[33,38,58] H can passivate dangling bonds removing those defects from the band gap. These defects are always the lowest energy configuration and in essence represent a healing of the network via the removal of undercoordinated centers. Their formation energies are negative with the chemical potential convention employed here and are thus favored regardless of the starting geometry. It is important to note that while energetically favored, the concentration of passivation sites is limited by the number of dangling bonds present in the pristine cell used for this study.

The insertion of H across strained Si–N bonds is found to provide a route for the H-induced defect formation and the disruption of the amorphous network. It constitutes an important atomistic mechanism for the experimentally observed H-induced softening of a-Si_3N_4.[23,43,44] While baring some similarities with the H-induced bond rupture seen in SiO_2, there are some important differences with the Si–H formation being favored as opposed to N-centered H defects. Both in this study and within a realistic a-Si_3N_4 film, H-insertion is naturally limited by the number of strained precursor sites. The further implication is that the strain present in the film as a result of the substrate or growth conditions will directly impact the H_{ins} concentration by influencing the number

Table 6.1: Simplified schematic overview of charge relaxation for both N- and Si-centered H defects for different (global) charge states q. e^- denotes intrinsic electron polaron, and h^+ an intrinsic hole trap. The N/Si–H bonds are presented as dative bonds (→) to describe the rearrangement of electrons upon H incorporation.

q	N–H			Si–H		
+1	$N + H^+$	⟶	$N{\rightarrow}H^+$	$Si + H^+$	⟶	$Si{\leftarrow}H^- + 2\,h^+$
0	$N + H^0$	⟶	$N{\rightarrow}H^+ + e^-$	$Si + H^0$	⟶	$Si{\leftarrow}H^- + h^+$
−1	$N + H^-$	⟶	$N{\rightarrow}H^+ + 2\,e^-$	$Si + H^-$	⟶	$Si{\leftarrow}H^-$

of precursor sites. The same argument can be extended for the distribution of precursor sites within a given film with more strained environments found in close proximity to the a-Si_3N_4-substrate interface(s) within a device stack.

The majority of H-defects interact with N/Si with intact coordination shells and sit in a broad range of formation energies with the $H_{i\text{-}N}$ (E^0_{form} = 1.81 eV) centers typically lower in energy than $H_{i\text{-}Si}$ and H_{bri} (E^0_{form} = 2.18 eV). The range of energy is largely dictated by the steric environment of the reference atom in the pristine situation before H incorporation. Perhaps most intriguingly, the CTLs sit in a narrow range for each of the main classes of H-defects for both centers ($H_{i\text{-}N}$, $H_{i\text{-}Si}$, H_{ins}). This very small spread of the CTLs across a range of defect configurations in stark contrast to their formation energetics seems puzzling at first glance. Examination of the nature of the defect states reveals the reason: In each case the H-configuration is independent of charge state. This is driven by the H-states sitting deep within the valence (and conduction) bands thereby playing no active role in charge trapping. Instead, they merely act as carriers of an initial electron or hole localizing in a charge trap state predetermined by pristine a-Si_3N_4, *i.e.,* at the h^+ and e^- trap sites were identified in Chapter 5. This is schematically summarized in Table 6.1.

In comparison, H incorporation is much more widely studied oxide system, where H forms amphoteric defects whose charge states are dictated by Fermi energy with the +/− CTLs sitting approximately 4.25 eV below the vacuum level.[48,51] In contrast, H-incorporation in a-Si_3N_4 is quite different, where the localized nature of the band-edges and the propensity for the system to trap electrons and holes results in the charging of the a-Si_3N_4 dielectric layer. In common with a-SiO_2, H in a-Si_3N_4 is found to facilitate the breaking of strained bonds. However, the mechanism is different: Rather than creating an analog of the hydroxylated E′,[53] H preferentially adds to the Si-site in the first instance. Equally, it is important to note that in the case of a-SiO_2 the charge trapping occurs at the center where the bond breaks, whereas in a-Si_3N_4 the charge is located on a trap site unrelated to the site of H-insertion.

At this juncture, it is important to raise two questions which go beyond the scope of this work. Firstly, how is H incorporation affected in Si- and N-rich SiN_x? This is important because tuning the stoichiometry is used to achieve application-specific performance of the material. In cases where deviations from stoichiometric a-Si_3N_4 are small, it would be reasonable to expect similar behavior as described here. However, when the deviations are

6

significant, new structural motifs might be introduced that are not captured by the present study. Secondly, how does the nature of the intrinsic trap sites and the range of levels previously described affect H incorporation? Both of these questions together with the impact of increasing the H concentration are currently under investigation.

6.3 Conclusion and Summary

In summary, the investigation of H-defect centers in a-Si_3N_4 uncovers the multifaceted role of H. While hydrogen has been known to passivate dangling bonds, thereby enhancing the electronic and optical properties playing the role of "Jekyll", while beyond passivation also its "Hyde" emerges: Incorporated H atoms instigate Si–N bond disruptions, especially in strained regions characterized by a distorted Si coordination environment and at least one elongated Si–N bond. It is noteworthy that the majority of hydrogen-associated states — whether from NH or most SiH configurations — reside within the valence and conduction bands, rendering them electronically inert. Charge trapping is predominantly linked to intrinsic traps for NH defects, and N-centers in the case of SiH defects, although a few high-energy H-configurations act as exceptions. The identification of an intrinsic electron bi-polaron in the -1 charge state for NH defects, which induces a significant relaxation in the amorphous network, requires further study. Importantly, this study bridges the understanding between H behaviors in a-SiO_2 and a-Si_3N_4 while emphasizing some important differences. It is plausible to infer — and left for future work to be confirmed — that analogous behavior could be seen in materials characterized by band edges that show a degree of localization.

6.4 Computational Details

Fermi energy and charge dependent defect formation energies $E_{\mathrm{form}}(E_{\mathrm{F}}; q)$ for incorporation of hydrogen into a-Si_3N_4 were calculated using the standard formalism of Zhang and Northrup[62] based on density functional theory (DFT) at the hybrid functional level. The chemical potential of H has been taken as $\frac{1}{2}H_2$. The defect formation energies for incorporation of hydrogen in the neutral charge state ($E^0_{\mathrm{form}} = E_{\mathrm{form}}(E_{\mathrm{F}}; 0)$) are generally re-

ferred to as *the* formation energies. By convention the charge transition level (CTL) is defined as the Fermi energy at which the formation energy of two charge states is equal ($E_{\text{form}}(q)-E_{\text{form}}(q') = 0$). Finite-size corrections for the charged systems are performed using the Lany-Zunger correction scheme.[63] All DFT calculations were performed spin polarised using the CP2K[64] code using the HSE06[65,66] exchange-correlation functional with the auxiliary density matrix method (ADMM).[67] The DZVP-SR-MOLOPT[68] family of basis-sets were employed to describe the valence electrons together with GTH-pseudopotentials[69–71] for the core electrons.

The problem of structure sampling was explored at length in Chapter 3 as it represents a vital consideration for amorphous systems. A single a-Si_3N_4 cell is selected to allow the problem of site sampling to be untangled from the broad range of intrinsic trap sites previously described. To achieve this the previous statistical sampling scheme is extended to the consideration of H-defects capturing the variety of geometries of the host lattice. This approach is presented in Section 3.4 resulting in selection of 60 seed sites for H incorporation, with 25 (35) originally centered at Si (N), respectively.

References

[1] Okada, A. *J. Eur. Ceram. Soc.* **2008**, *28*, 1097–1104.

[2] Doo, V. Y.; Nichols, D. R.; Silvey, G. A. *J. Electrochem. Soc.* **1966**, *113*, 1279.

[3] Tsai, S.-J.; Wang, C.-L.; Lee, H.-C.; Lin, C.-Y.; Chen, J.-W.; Shiu, H.-W.; Chang, L.-Y.; Hsueh, H.-T.; Chen, H.-Y.; Tsai, J.-Y., et al. *Sci. Rep.* **2016**, *6*, 28326.

[4] Törmä, P. T.; Sipilä, H. J.; Mattila, M.; Kostamo, P.; Kostamo, J.; Kostamo, E.; Lipsanen, H.; Nelms, N.; Shortt, B.; Bavdaz, M.; Laubis, C. *IEEE Trans. Nuc. Sci.* **2013**, *60*, 1311–1314.

[5] Törmä, P. T.; Kostamo, J.; Sipilä, H.; Mattila, M.; Kostamo, P.; Kostamo, E.; Lipsanen, H.; Laubis, C.; Scholze, F.; Nelms, N.; Shortt, B.; Bavdaz, M. *IEEE Trans. Nuc. Sci.* **2014**, *61*, 695–699.

[6] Cornaby, S.; Bilderback, D. H. *J. Sync. Rad.* **2008**, *15*, 371–373.

[7] Sharma, T.; Wang, J.; Kaushik, B. K.; Cheng, Z.; Kumar, R.; Wei, Z.; Li, X. *IEEE Access* **2020**, *8*, 195436–195446.

[8] Xiang, C.; Jin, W.; Bowers, J. E. *Photonics Res.* **2022**, *10*, A82–A96.

[9] Goldfarb, D. L. In *Photomask Technology 2015*, ed. by Hayashi, N.; Kasprowicz, B. S., SPIE: Monterey, California, United States, 2015, 96350A.

[10] Pollentier, I.; Lee, J. U.; Timmermans, M.; Adelmann, C.; Zahedmanesh, H.; Huyghebaert, C.; Gallagher, E. E. In *Extreme Ultraviolet (EUV) Lithography VIII*, ed. by Panning, E. M., SPIE: 2017; Vol. 10143, p 101430L.

[11] Van de Kerkhof, M.; Yakunin, A. M.; Kvon, V.; Nikipelov, A.; Astakhov, D.; Krainov, P.; Banine, V. *Radiat. Eff. Defect. S.* **2022**, *177*, 486–512.

[12] Zhang, J.; Liu, G.; Cui, W.; Ge, Y.; Du, S.; Gao, Y.; Zhang, Y.; Li, F.; Chen, Z.; Du, S., et al. *Science* **2022**, *378*, 371–376.

[13] Liu, N.; Yang, X.; Zhu, Z.; Chen, F.; Zhou, Y.; Xu, J.; Liu, K. *Nanoscale* **2022**, *14*, 49–54.

[14] Aiyama, T.; Fukunaga, T.; Niihara, K.; Hirai, T.; Suzuki, K. *J. Non-Cryst. Solids* **1979**, *33*, 131–139.

[15] Misawa, M.; Fukunaga, T.; Niihara, K.; Hirai, T.; Suzuki, K. *J. Non-Cryst. Solids* **1979**, *34*, 313–321.

6

[16] Wakita, K. W. K.; Hayashi, H. H. H.; Nakayama, Y. N. Y. *Jpn. J. Appl. Phys.* **1996**, *35*, 2557.

[17] Deshpande, S. V.; Gulari, E.; Brown, S. W.; Rand, S. C. *J. Appl. Phys.* **1995**, *77*, 6534–6541.

[18] Sahu, B. S.; Delachat, F.; Slaoui, A.; Carrada, M.; Ferblantier, G.; Muller, D. *Nanoscale Res. Lett.* **2011**, *6*, 1–10.

[19] Gritsenko, V. A.; Kruchinin, V. N.; Prosvirin, I. P.; Novikov, Y. N.; Chin, A.; Volodin, V. A. *J. Exp. Theor. Phys.* **2019**, *129*, 924–934.

[20] Robertson, J. *Appl. Phys. Lett* **1991**, *59*, 3425–3427.

[21] Warren, W. L.; Robertson, J.; Kanicki, J. *Appl. Phys. Lett* **1993**, *63*, 2685–2687.

[22] Krick, D. T.; Lenahan, P. M.; Kanicki, J. *Phys. Rev. B* **1988**, *38*, 8226–8229.

[23] Hasegawa, S.; Amano, Y.; Inokuma, T.; Kurata, Y. *J. Appl. Phys.* **1994**, *75*, 1493–1500.

[24] Martınez, F. L.; del Prado, A.; Martil, I.; Gonzalez-Dıaz, G.; Selle, B.; Sieber, I. *J. Appl. Phys.* **1999**, *86*, 2055–2061.

[25] Roizin, Y. *J. Non.-Cryst. Solids* **1991**, *137-138*, 61–64.

[26] Bommali, R. K.; Ghosh, S.; Vijaya Prakash, G.; Gao, K.; Zhou, S.; Khan, S. A.; Srivastava, P. *J. Appl. Phys.* **2014**, *115*, 053525.

[27] Zoldesi, C. et al. In ed. by Wood, O. R.; Panning, E. M., San Jose, California, United States, 2014, 90481N.

[28] Warren, W. L.; Lenahan, P. M. *Phys. Rev. B* **1990**, *42*, 1773–1780.

[29] Warren, W. L.; Lenahan, P. M.; Curry, S. E. *Phys. Rev. Lett.* **1990**, *65*, 207–210.

[30] Warren, W.; Kanicki, J.; Rong, F.; Poindexter, E. *J. Electrochem. Soc.* **1992**, *139*, 880.

[31] Warren, W.; Robertson, J.; Kanicki, J. *Appl. Phys. Lett.* **1993**, *63*, 2685–2687.

[32] Warren, W. L.; Kanicki, J.; Poindexter, E. H. *Colloids Surf. A: Physicochem. Eng. Asp.* **1996**, *115*, 311–317.

[33] Di Valentin, C.; Palma, G.; Pacchioni, G. *J. Phys. Chem. C* **2011**, *115*, 561–569.

[34] Hintzsche, L.; Fang, C.; Watts, T.; Marsman, M.; Jordan, G.; Lamers, M.; Weeber, A.; Kresse, G. *Phys. Rev. B* **2012**, *86*, 235204.

[35] Kroll, P. *J. Non-Cryst. Solids* **2001**, *293-295*, 238–243.

[36] Choi, W. I.; Son, W.-J.; Dronskowski, R.; Oh, Y.; Yang, S.-Y.; Kwon, U.; Kim, D. S. *Adv. Mater.* **2024**, *36*, 2308054.

[37] Rehman, A.; van de Kruijs, R. W. E.; van den Beld, W. T. E.; Sturm, J. M.; Ackermann, M. *J. Phys. Chem. C* **2023**, *127*, 17770–17780.

[38] Wilhelmer, C.; Waldhoer, D.; Cvitkovich, L.; Milardovich, D.; Waltl, M.; Grasser, T. *Nanomaterials* **2023**, *13*, 2286.

[39] Mártil, I.; del Prado, A.; San Andrés, E.; González Dıáz, G.; Martınez, F. L. *J. Appl. Phys.* **2003**, *94*, 2642–2653.

[40] San Andrés, E.; Del Prado, A.; Martınez, F.; Mártil, I.; Bravo, D.; López, F. *J. Appl. Phys.* **2000**, *87*, 1187–1192.

[41] Warren, W. L.; Kanicki, J.; Robertson, J.; Poindexter, E. H.; McWhorter, P. J. *J. Appl. Phys.* **1993**, *74*, 4034–4046.

[42] Song, C.; Huang, R.; Wang, X.; Guo, Y.; Song, J.; Zhang, Y.; Zheng, Z. *Appl. Surf. Sci.* **2011**, *258*, 1290–1293.

[43] Lindley, M.; Elias, D.; Jones, B.; Pitman, K. *J. Mater. Sci.* **1979**, *14*, 70–85.

[44] Laarz, E.; Zhmud, B. V.; Bergström, L. *J. Am. Ceram. Soc.* **2000**, *83*, 2394–400.

[45] Van de Walle, C. G.; Denteneer, P. J. H.; Bar-Yam, Y.; Pantelides, S. T. *Phys. Rev. B* **1989**, *39*, 10791–10808.

[46] Neugebauer, J.; Van de Walle, C. G. *Phys. Rev. Lett.* **1995**, *75*, 4452–4455.

[47] Van de Walle, C. G. *Phys. Rev. Lett.* **2000**, *85*, 1012–1015.

[48] De Walle, C. V.; Neugebauer, J. *Nature* **2003**, *423*, 626–628.

[49] Robertson, J.; Peacock, P. *Thin Solid Films* **2003**, *445*, Proceedings of the 3rd International Symposium on Transparent Oxide Thin films for Electronics and Optics, 155–160.

[50] Xiong, K.; Robertson, J.; Clark, S. J. *J. Appl. Phys.* **2007**, *102*, 083710.

[51] Li, H.; Robertson, J. *J. Appl. Phys.* **2014**, *115*, 203708.

[52] Godet, J.; Pasquarello, A. *Microelectronic Eng.* **2005**, *80*, 14th biennial Conference on Insulating Films on Semiconductors, 288–291.

[53] El-Sayed, A.-M.; Watkins, M. B.; Grasser, T.; Afanas'ev, V. V.; Shluger, A. L. *Phys. Rev. Lett.* **2015**, *114*, 115503.

[54] El-Sayed, A.-M.; Wimmer, Y.; Goes, W.; Grasser, T.; Afanas'ev, V. V.; Shluger, A. L. *Phys. Rev. B* **2015**, *92*, 014107.

[55] Wilhelmer, C.; Waldhoer, D.; Jech, M.; El-Sayed, A.-M. B.; Cvitkovich, L.; Waltl, M.; Grasser, T. *Microelectron. Reliab.* **2022**, *139*, 114801.

[56] Griggs, D. *Geophys. J. Int.* **1967**, *14*, 19–31.

[57] Herrmann, M. *J. Am. Ceram. Soc.* **2013**, *96*, 3009–3022.

[58] Grillo, M.-E.; Elliott, S. D.; Freysoldt, C. *Phys. Rev. B* **2011**, *83*, 085208.

[59] Martin, J. M. L.; Lee, T. J.; Taylor, P. R. *J. Chem. Phys.* **1992**, *97*, 8361–8371.

[60] Boyd, D. R. J. *J. Chem. Phys.* **1955**, *23*, 922–926.

[61] Wimmer, Y.; El-Sayed, A.-M.; Gös, W.; Grasser, T.; Shluger, A. L. *Proc. Math. Phys. Eng. Sci.* **2016**, *472*, 20160009.

[62] Zhang, S. B.; Northrup, J. E. *Phys. Rev. Lett.* **1991**, *67*, 2339–2342.

[63] Lany, S.; Zunger, A. *Model. Simul. Mat. Sci. Eng.* **2009**, *17*, 084002.

[64] Kühne, T. D. et al. *J. Chem. Phys.* **2020**, *152*, 194103.

[65] Heyd, J.; Scuseria, G. E.; Ernzerhof, M. *J. Chem. Phys.* **2003**, *118*, 8207–8215.

[66] Heyd, J.; Scuseria, G. E.; Ernzerhof, M. *J. Chem. Phys.* **2006**, *124*, 219906.

[67] Guidon, M.; Hutter, J.; VandeVondele, J. *J. Chem. Theor. and Comp.* **2010**, *6*, 2348–2364.

[68] VandeVondele, J.; Hutter, J. *J. Chem. Phys.* **2007**, *127*, 114105.

[69] Goedecker, S.; Teter, M.; Hutter, J. *Phys. Rev. B* **1996**, *54*, 1703–1710.

[70] Hartwigsen, C.; Goedecker, S.; Hutter, J. *Phys. Rev. B* **1998**, *58*, 3641–3662.

[71] Krack, M. *Theor. Chem. Acc.* **2005**, *114*, 145–152.